Synthesis and characterization of FePd magnetic nanoparticles modified with chiral BINAP ligand as a recoverable catalyst vehicle for the asymmetric coupling reaction

Kohsuke Mori, Yuichi Kondo and Hiromi Yamashita*

Received 21st May 2009, Accepted 26th June 2009
First published as an Advance Article on the web 30th July 2009
DOI: 10.1039/b910069e

The initial thermal decomposition of iron carbonyl ($Fe(CO)_5$), followed by reduction of palladium acetylacetonate ($Pd(acac)_2$) produced FePd nanoparticles (NPs) with an Fe_xO_y-rich core and a Pd-rich shell. The as-synthesized NPs were subsequently treated with (*S*)-2,2′-bis(diphenylphosphino)-1,1′-binaphthene ((*S*)-BINAP) as a chiral modifier, which provides them with the optical activity to show a negative Cotton effect in the circular dichroism (CD) spectrum. Characterization by means of X-ray diffraction (XRD), transmission electron microscopy (TEM), superconducting quantum interface device (SQUID) and X-ray absorption fine structure (XAFS) measurements was performed. The FePd NPs modified with (*S*)-BINAP had a mean diameter of *ca.* 5.6 nm, and exhibited superparamagnetic behavior at 300 K with zero remanence and coercivity. The FePd-(*S*)-BINAP was shown to catalyze the asymmetric Suzuki–Miyaura coupling reaction with easy recovery from the reaction mixture by applying an external magnet. The designed architecture enabled the powerful combination of two functionalities, magnetism that responds to a magnetic field for easy recycling, as well as an optically active catalytic center that promotes the asymmetric coupling reaction.

Introduction

Nanoscale metal particles are gaining increasing attention in the field of catalysis, nanoelectronics, and material science because of their existence on borderline molecular states with discrete quantum energy levels.[1] Thus, nanoparticle (NP)-based catalysts are considered to bridge the gap between mononuclear metal complexes and heterogeneous bulk catalysts. Their large surface area-to-volume ratio allows effective utilization of expensive metals. The variation in primary structures, such as size, composition, morphology and protective ligand allows precise control of catalytic activities.[2] Promising synthetic methods providing suitable NPs responsible for target catalytic reactions are extremely important.[3] NP-based catalysts are key components of catalytic activities; however, their application in liquid suspensions is limited due to the difficulty in product separation and catalyst recycling. In order to overcome the above drawbacks, catalytic NPs have generally been immobilized on solid supports (*e.g.*, carbon, metal oxides, and zeolites) or stabilized by capping with ligands ranging from small organic molecules to large polymers.[4] Recently, novel systems such as dendrimers,[5] block copolymer nanospheres[6] and cross-linked lyotropic liquid crystals[7] were employed to encapsulate metal NPs.

Alternatively, superparamagnetic NPs are a new type of soluble matrix that can potentially address the isolation and recycling problems encountered in nano-sized catalysts.[8] For example, we have recently developed Ti-containing silica ($Ti\text{-}SiO_2$) encapsulating superparamagnetic fcc FePt NPs ($FePt@Ti\text{-}SiO_2$).[8d] The inner magnetic FePt cores were shielded from the external environment by the impermeable coating, which prevents sintering and agglomeration of metal NPs under catalytic conditions. The catalytically active Ti-oxide moieties are located on the external surface of the coating and considered to be highly dispersed at the atomic level. Although there have been some developments on the use of magnetic NPs to host soluble catalytically active organometallic complexes and enzymes;[9] the use of NP itself as a catalytically active species has rarely been explored.

Herein, we present a chiral BINAP-modified FePd magnetic NP exhibiting asymmetric catalytic activities. The FePd NP was synthesized by the thermal decomposition of iron carbonyl ($Fe(CO)_5$) and subsequent reduction of palladium acetylacetonate ($Pd(acac)_2$) in the presence of oleic acid and oleylamine with the aim of producing Fe_xO_y-rich core and Pd-rich shell. Such NPs have been modified with chiral 2,2′-bis(diphenylphosphino)-1,1′-binaphthene (BINAP) through the simple ligand exchange procedure, which successfully offer a platform to catalyze Pd-based asymmetric catalytic reactions. The BINAP ligands also act as stabilizer of the inner magnetic NPs, which prevent sintering and agglomeration under catalytic conditions. The present $Fe_{core}Pd_{shell}$ NPs possess other attractive features compared to the single Pd component-based systems. Firstly, the replacement of the interior of precious Pd NPs with inexpensive core metals contribute to the atomic economy. Secondly, the magnetic core provides an opportunity for achieving the convenient separation of the nanocatalyst after

Division of Materials and Manufacturing Science, Graduate School of Engineering, Osaka University, 2-1 Yamada-oka, Suita, Osaka 565-0871. E-mail: yamashita@mat.eng.osaka-u.ac.jp; Fax: +81 (0)6 6879 7457; Tel: +81 (0)6 6879 7457

catalytic reaction by applying an external magnet. This study represents the first step in the possible application of BINAP-modified magnetic NP as a novel chiral nanocatalyst.

Results and discussion

Bimetallic NPs, such as FePt and FePd, are commonly synthesized *via* co-reduction of an iron salt and platinum or palladium acetylacetonate in the presence of oleic acid and oleylamine, which act as ligands to stabilize NPs.[10] For the structural model of as-synthesized bimetallic NPs, it is reasonable to suggest that most of the Pt or Pd atoms are preferentially located in the core region, while the Fe atoms are preferentially located in the shell region.[11] Since the reduction potentials of Pt and Pd ions are more positive than Fe ions ($E^0(Pt^{2+}/Pt^0) = +1.2$ V, $E^0(Pd^{2+}/Pd^0) = +0.63$ V, $E^0(Fe^{2+}/Fe^0) = -0.44$ V *vs.* NHE), the former are reduced first and constitute the core. This is followed by the reduction of Fe ions on the surface of the Pt or Pd core. However, such NPs having an Fe-rich shell are thought to be inappropriate for application to catalytic reactions based on transition metals.

With this in mind, we controlled the composition of FePd NPs to form a $Fe_{core}Pd_{shell}$ by applying successive reduction of metal precursors as follows. At first, $Fe(CO)_5$ was mixed with dibenzyl ether and the mixture heated to 523 K under Ar with vigorous mechanical stirring to form the Fe core. Next, $Pd(acac)_2$, oleic acid and oleylamine were then injected with mechanical stirring, and then the reaction mixture was heated at a rate of ~ 5 K min^{-1} to 583 K and kept stirring for 1 h. The resulting NPs were precipitated with excess ethanol and collected by centrifugation. Elemental analysis confirmed that the average composition of the NPs was $Fe_{60}Pd_{40}$.

To explore the possibility to attain asymmetric catalytic reactions on active NPs, the modification with chiral BINAP was performed (Fig. 1). The mixture of a toluene suspension of NPs and chiral BINAP was stirred vigorously at 353 K. After

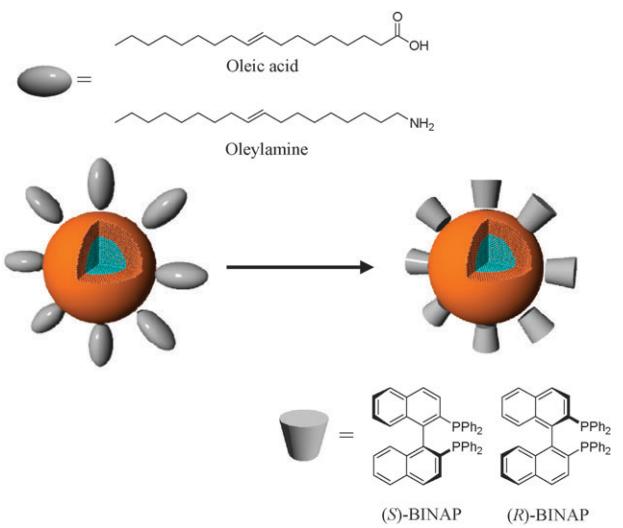

Fig. 1 Ligand exchange procedure of FePd NP from oleic acid/oleylamine to chiral BINAP. The dense core is Fe rich and the pale shell is Pt rich.

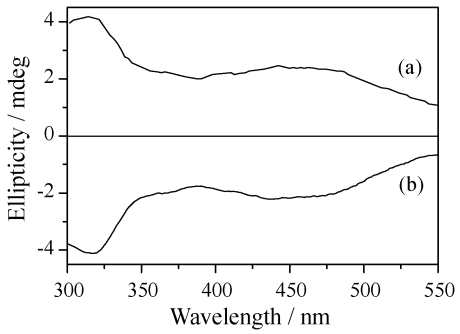

Fig. 2 Circular dichroism (CD) spectra of FePd NPs stabilized by (a) (*R*)-BINAP and (b) (*S*)-BINAP in $CHCl_3$.

stirring for 24 h, the NPs were collected by centrifugation and washed several times with toluene. The composition of Fe and Pd remained unchanged after the modification with BINAP. In the FT-IR spectrum, the peaks due to the methylene ν(C–H) stretch vibration of oleic acid and/or oleylamine at around 3000–3100 cm^{-1} disappeared, accompanied with the appearance of the aromatic ring ν(C–H) stretch vibration of BINAP ligand at around 2800–3000 cm^{-1}. The circular dichroism (CD) spectra of (*S*)-BINAP-modified NPs in $CHCl_3$ showed negative cotton effect in the 300–550 nm spectral range, while (*R*)-BINAP-modified NPs showed positive cotton effects, as exhibited in Fig. 2.[12] These NPs were stable against racemization. It can be said that the new optically active NPs in which the chiral center is very close to the surface of the NPs can be obtained through the simple ligand exchange procedure. These NPs are also expected to be a single magnetic domain and exhibit a magnetic moment only in the presence of a magnetic field, indicating a superparamagnetic nature. When the magnetic field is removed, the particles immediately return to their nonmagnetic state.

In the XRD pattern of the FePd NPs stabilized with (*S*)-BINAP, the intensities of the diffraction peaks are low, presumably due to the smaller size of the particles (Fig. 3b). However, they exhibited clear peaks due to the fcc Pd at around 40.0°, 46.7° and 68.5°, corresponding to the (111), (200), and (220) reflections, respectively. The peak also involves γ-Fe_2O_3 and/or Fe_3O_4 phases (Fe_xO_y) at around 30.3°, 35.7°, 57.3° and 63.0°, corresponding to the (220), (300), (511) and (440) reflections, respectively. The average

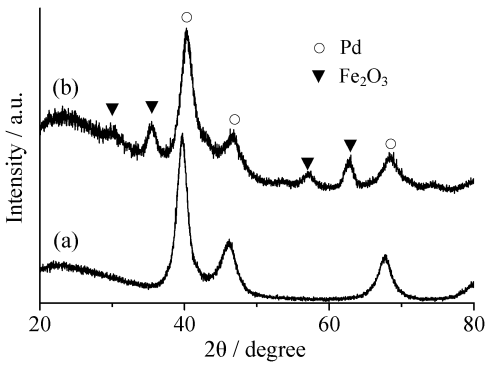

Fig. 3 XRD pattern of (a) Pd NPs and (b) FePd NPs stabilized by (*S*)-BINAP.

crystalline size of the Fe_xO_y phase was calculated to be 4.7 nm by applying Scherrer's equation for the (311) reflection. Distinguishing between the γ-Fe_2O_3 and Fe_3O_4 phase by XRD is quite difficult because of the same inverse spinel structure and similarity in their d spacing.[13] However, due to similar magnetic properties of γ-Fe_2O_3 and Fe_3O_4, it is not necessary to identify the percentage of each phase. Note that the position of (111) peak in FePd NPs showed an obvious shift to the higher angle compared to the pure Pd NPs (Fig. 3a *vs.* b), suggesting the formation of FePd phase.[14]

Fig. 4a and b shows a transmission electron microscopy (TEM) image and size distribution diagram. The FePd NPs, having an average diameter (d_{ave}) of *ca.* 5.6 nm, were found to be distributed within the image area (standard deviation: σ = 1.6 nm, σ/d = 28.6%). The diffraction patterns exhibited atomic lattice fringes corresponding to the (111), (200), (220) and (113) planes of the fcc structure of the Pd NP, respectively (Fig. 4c). Assuming that the present NP is a core–shell structure with a spherical shape, the diameters of the Fe_xO_y core and Pd shells were determined to be 4.7 nm and 0.9 nm, respectively. The thickness of the Pd shell corresponds to about 4 layers of Pd. A particle size of 5.6 nm is suitable for achieving a high surface area of Pd while keeping strong magnetism. It is desirable to minimize the amount of Pd as much as possible for economic reason. On the contrary, if the size of Fe_xO_y core is less than 2 nm, such small Fe_xO_y core does not have a strong enough magnetism for magnetic recycling process.

The magnetic properties were investigated using a superconducting quantum interface device (SQUID) magnetometer (Fig. 5). The isothermal magnetization curve at 300 K displayed a rapid increase with increasing applied magnetic field, due to superparamagnetic relaxation.[15] This indicates that the thermal energy can overcome the anisotropy energy barrier of the individual particles, and the net magnetization of these nanoparticle assemblies is zero in the absence of an external field. Hysteresis was absent with zero remanence (M_r) and coercivity (H_c), and the saturation magnetization (M_s) reached up to 19.0 emu g^{-1}. With decreasing temperature, the magnetization increased and exhibited a symmetric hysteresis loop at 5 K (M_r = 6.1 emu g^{-1}, H_c = 190 Oe), indicating a transition from superparamagnetic to ferromagnetic behavior.

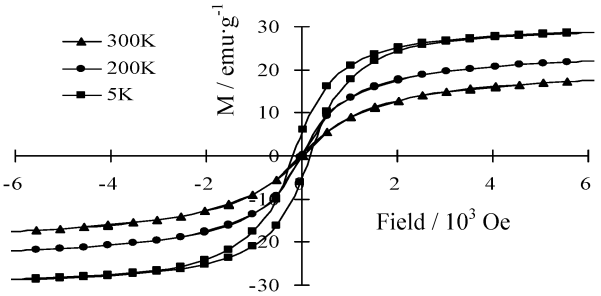

Fig. 5 Field-dependent magnetization curve for FePd NPs stabilized by (*S*)-BINAP measured at 300 K (■), 200 K (●) and 5 K (▲).

X-Ray absorption measurement was carried out to elucidate the electronic structure and chemical environment of the $Fe_{core}Pd_{shell}$ NPs modified with (*S*)-BINAP. In comparison, the FePd NPs was also prepared by the conventional co-reduction method with the intension of producing $Fe_{shell}Pd_{core}$ NPs. Fig. 6A shows the normalized X-ray absorption near-edge structure (XANES) spectra at the Pd K-edge of both FePd NPs as well as standard samples including Pd foil and PdO. The absorption edge varies with respect to the oxidation state of the palladium, and the XANES spectrum of the PdO has one broad peak at around 24 365 eV, while Pd foil showed two distinct peaks at around 24 350 and 24 370 eV, corresponding to the allowed 1s → 5p transition. The shapes of the XANES spectra and the edge position of both FePd NPs resembled those of Pd foil, but differed from those of PdO, suggesting that the oxidation state of Pd in the FePd samples was almost Pd^0. More detailed inspection revealed that two characteristic peaks in the $Fe_{core}Pd_{shell}$ NPs seem a

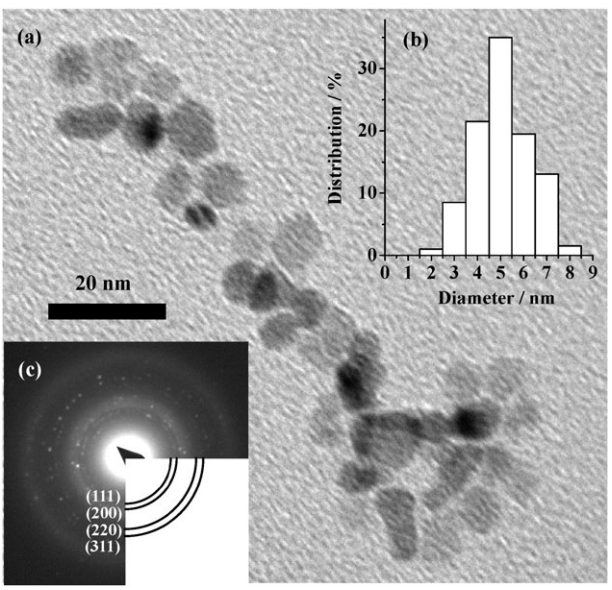

Fig. 4 (a) TEM image, (b) size distribution diagram and (c) electron diffraction pattern of FePd NPs stabilized by (*S*)-BINAP.

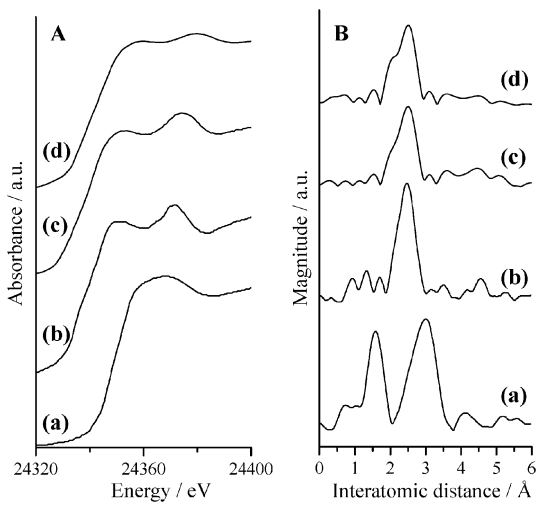

Fig. 6 (A) Pd K-edge XANES spectra and (B) FT-EXAFS spectra for (a) PdO, (b) Pd foil, (c) FePd NPs prepared by conventional co-reduction method and stabilized by (*S*)-BINAP, and (d) FePd NPs stabilized by (*S*)-BINAP.

little weak, compared to the $Fe_{shll}Pd_{core}$ NPs prepared by the conventional co-reduction method. This indicates that the symmetry of the Pd metal fcc structure in the shell region is slightly disordered due to the exposure to the surface. Fig. 6B shows the Fourier transforms (FT) of Pd K-edge extended X-ray absorption fine structure (EXAFS) spectra of these samples. FePd samples exhibited a single peak at approximately 2.5 Å, which could be assigned to the contiguous Pd–Pd bond in the metallic form. The Pd–Pd distance in both FePd samples, however, accompanied the shouldered peak at around 2.2 Å, suggesting the presence of Fe–Pd heteroatomic bonding. No peaks due to Pd–O and Pd–O–Pd bonds, detectable in that of PdO at around 1.6 and 3.0 Å, were observed.

Fig. 7A shows the Fe K-edge XANES spectra of both FePt NPs and reference iron compounds. The edge position (measured at the half-height of the edge jump) depends on the electronic charge of the iron ion, and the energy increased in the order of Fe foil (7117.1 eV) < $Fe_{core}Pd_{shell}$ NPs (7118.0 eV) < $Fe_{shell}Pd_{core}$ NPs (7119.0 eV) < Fe_2O_3 (7122.0 eV). Thus, the iron elements in the $Fe_{shell}Pd_{core}$ NPs are more oxidized than those of the $Fe_{core}Pd_{shell}$ NPs because of their exposure to the surface. The FT-EXAFS spectra of the FePd samples demonstrated a peak between 1.5 and 2.9 Å, corresponding to the Fe–O and Fe–O–Fe bonds, accompanied with a slight peak at around 2.1 Å corresponding to the Fe–Fe bond (Fig. 7B). Compared to the Fe_2O_3 and $Fe_{shell}Pd_{core}$ NPs, the intensity of the second peaks for the $Fe_{core}Pd_{shell}$ NPs is significantly weakened. This peak is attributable to the contiguous Fe–O–Fe bonds due to face-, edge-, vertex-sharing FeO_6 octahedra. The reduced intensity of the $Fe_{core}Pd_{shell}$ NPs in this region can be explained by the structural disorder in the extremely small NPs.[8c,16] The iron oxide particles in the core region are responsible for the weakness of the high order coordination shell. For the structural model of the $Fe_{core}Pd_{shell}$ NPs, the overall results suggest that most of the Pd atoms are preferentially located in the shell region, the Fe atoms are preferentially located in the core region.

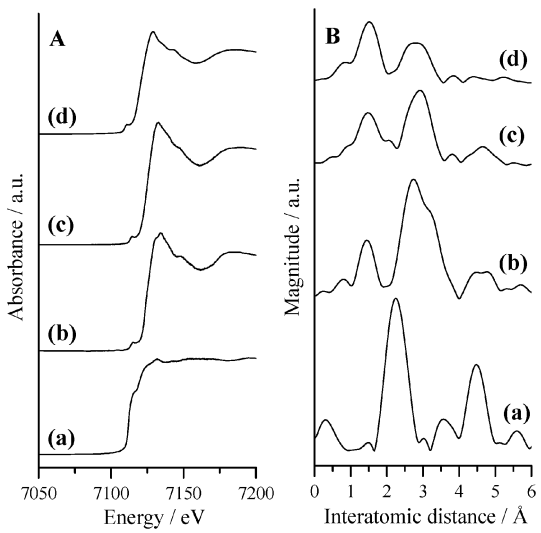

Fig. 7 (A) Fe K-edge XANES spectra and (B) FT-EXAFS spectra for (a) Fe foil, (b) Fe_2O_3, (c) FePd NPs prepared by conventional co-reduction method and stabilized by (*S*)-BINAP, and (d) FePd NPs stabilized by (*S*)-BINAP.

The above XRD and XAFS results clearly suggest that the iron atoms exist in an oxide phase. The fact that no iron signal in the XRD and XAFS measurements suggests that $Fe(CO)_5$ decomposition was accompanied by the oxidation iron either during the high-temperature reaction and/or the subsequent steps. The oxidation of Fe-containing NPs of alloy has been reported previously.[17]

Palladium-mediated cross-coupling reactions between aryl halides and nucleophiles, exemplified by Suzuki–Miyaura coupling reactions, have received considerable attention due to their enormous synthetic potential to form new carbon–carbon bonds.[18] New classes of Pd complexes having Pd–carbon σ bonds, *e.g.* palladacycle complexes,[19] PCP pincer-type complexes[20] and *N*-heterocyclic carbenes (NHCs),[21] have led to significant breakthroughs in this area. The extension to an asymmetric version between naphthyl halide and naphthylboronic acid catalyzed by chiral Pd–phosphine complexes[22] and chiral Pd NPs[23] have gained popularity as an attractive methodology to produce axially chiral binaphthalenes. These compounds constitute a central building block in a large number of natural products. From practical and economical considerations, however, the demand for easily recoverable catalytic systems is extremely high in order to circumvent the drawbacks imposed by homogeneous Pd complexes. To the best of our knowledge, there have been no reports of the asymmetric Suzuki–Miyaura coupling reaction of naphthyl halide and naphthylboronic acid by a recoverable catalytic system so far.

The potential catalytic properties of the FePd NPs modified with chiral BINAP ligands were evaluated in the Suzuki–Miyaura coupling reaction of 1-bromo-2-methylnaphthylene (**1**) and 1-naphthylboronic acid (**2**) in DMF–H_2O solvent at 353 K (Scheme 1). It was found that the FePd NPs modified with (*S*)-BINAP served as a chiral nanocatalyst to afford the corresponding (*S*)-binaphthalene (**3**) in >99% yield with a moderate enantioselectivity of 48%. Since Fe atoms do not accelerate the above coupling reaction, our FePd NPs are thought to consist of an Fe-rich core and Pd-rich shell. No enantioselectivity was observed in the presence of the unmodified FePd NPs stabilized by OA/OAm. In the case of (*R*)-BINAP, (*R*)-binaphthalene was obtained with the same level of chemical yield and enantioselectivity, revealing that the absolute configuration of the coupling products is determined by the employed ligands. Periodic monitoring of the coupling reaction showed no induction period or

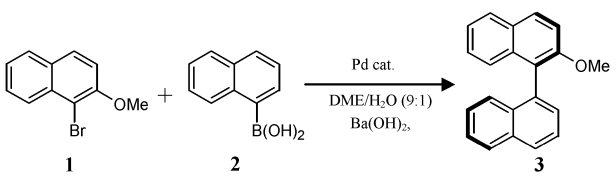

	Conv. / %	Ee / %
FePd-(*S*)-BINAP	> 99%	48
FePd-(*R*)-BINAP	>99%	46

Scheme 1

degradation: the enantioselectivity appeared to be independent of the conversion level and remained unchanged during the reaction, suggesting that racemization of the product did not take place. An important advantage of the FePd NPs with chiral BINAP is the facile recovery from the reaction mixture and the reusability. Upon completion of the reaction, the magnetic properties of the NPs can afford a straightforward means to isolate from the colloidal solution. By applying an external permanent magnet (surface magnetic flux density: 4500 G), the NPs were attracted within a few minutes. The recovered FePd NPs with BINAP could then be recycled while maintaining identical enantioselectivity in the absence of an externally added chiral ligand. In the reaction of **1** and **2**, the nanocatalyst was removed after 50% conversion, at the reaction temperature, followed by addition of $Ba(OH)_2$ to the filtrate and further reaction at 353 K (hot leaching test). The coupling reaction hardly occurred after catalyst removal. Thus, the asymmetric Suzuki–Miyaura coupling reaction undoubtedly proceeds on the chiral NPs' surface. Our bottom-up construction approach combined the advantages of the individual building blocks; the magnetic property of the Fe oxide core that is attracted to a magnetic field and the catalytic ability of the Pd shell for coupling reactions.

Conclusion

The first example of an asymmetric catalytic application using chiral magnetic FePd NPs was presented. The as-synthesized achiral FePd NPs stabilized by oleic acid and oleylamine were transferred into the chiral ones by a simple liquid-phase ligand exchange procedure with (*R*)- or (*S*)-BINAP, as demonstrated by CD spectra. Characterization by other physicochemical methods revealed superparamagnetic NPs with an average diameter of 5.6 nm. It was also proven that most of the Pd atoms existed in a metallic form, while the Fe atoms existed in an oxidized form. The resulting FePd NPs showed a catalytic activity for the enantioselective Suzuki–Miyaura coupling reaction, and the separation of these nanocatalysts in an external magnetic field can be achieved. The present strategy provides great flexibility in the selection of the magnetic core, catalytically active center and organic ligand for the target catalytic transformations.

Experimental

The synthesis of FePd NPs. FePd NPs were prepared using a Schlenk line by airless techniques. Iron pentacarbonyl (1.0 mmol, $Fe(CO)_5$, Aldrich) was mixed with 100 mL of dibenzyl ether (Tokyo Kasei Kogyo Co., Ltd) in a 500 mL three-neck flask. The mixture was degassed for 1 h and then heated to 523 K under Ar with vigorous mechanical stirring for 10 min. Palladium acetylacetonate (0.5 mmol, $Pd(acac)_2$, Wako Pure Chemical Ind., Ltd.), 2.5 mmol of oleic acid (Wako Pure Chemical Ind., Ltd.), and 2.5 mmol of oleylamine (Aldrich) dissolved in dibenzyl ether (5 mL) were then injected with mechanical stirring. The reaction mixture was heated at a rate of $\sim$5 K min^{-1} to 583 K and maintained for 1 h. The black colored solution was allowed to cool to room temperature and NPs were precipitated with excess ethanol and collected by centrifugation. After washing several times with toluene and ethanol, the precipitate was uniformly dispersed in toluene.

The modification procedure of the FePd NPs with BINAP. The modification was conducted by vigorous stirring of the mixture of toluene suspension of FePd NPs (0.5 mg particle mL^{-1}) and chiral BINAP (Tokyo Kasei Kogyo Co., Ltd.) at 353 K. After stirring for 3 h, the NPs were collected by centrifugation. After washing several times with toluene, the precipitate was dried under vacuum.

Characterization. X-Ray diffraction patterns were recorded using a Rigaku Mini-flex using Cu Kα radiation of wavelength 1.5418 Å. Elemental analysis was performed with EDX-720 (Shimadzu). Infrared spectra were obtained with a JASCO FTIR-6100. Samples were diluted with KBr and compressed into thin disk-shaped pellets. TEM micrographs were obtained with a Hitachi Hf-2000 FE-TEM equipped with a Kevex energy-dispersive X-ray detector operated at 200 kV. The magnetic properties were measured with a Quantum Design MPMS-XL. Fe K-edge and Pd K-edge XAFS spectra were recorded at room temperature in fluorescence mode at the beam line 01B1 station with an attached Si(311) monochromator at SPring-8, JASRI, Harima, Japan (prop. No. 2008A1366, 2008A1457). In a typical experiment, the sample was loaded into the *in situ* cell with plastic windows. The EXAFS data were examined using an EXAFS analysis program, Rigaku EXAFS. The pre-edge peaks in the XANES regions were normalized for atomic absorption, based on the average absorption coefficient of the spectral region. Fourier transformation (FT) of k^3-weighted normalized EXAFS data was performed over the 3.0 Å $< k/Å^{-1} <$ 12 Å range for Fe K-edge sample and 3.5 Å $< k/Å^{-1} <$ 12 Å range for Pd K-edge sample to obtain the radial structure function.

A typical example for the Suzuki–Miyaura coupling. Into a reaction vessel (50 mL) with a reflux condenser were placed FePd-(*S*)-BINAP (10 mg), 2-methoxynaphthyl bromide (0.5 mmol), 1-naphthylboronic acid (0.75 mmol), $Ba(OH)_2$ (1.5 mmol), and DME–H_2O (3 mL, DME : H_2O = 9 : 1). The resulting mixture was reacted at 353 K for 24 h under Ar atmosphere with magnetic stirring. The conversion and ee were determined by HPLC (Daicel Chiralcel OJ-H, *n*-hexane–2-propanol = 4 : 1 (v/v), 1.0 mL min^{-1}, 303 K, 272 nm, t_S = 8.0 min, t_R = 13.7 min).

Acknowledgements

The authors appreciate Dr Eiji Taguchi and Prof. Hirotaro Mori at the Research Center for Ultra-High Voltage Electron Microscopy, Osaka University for assistance with TEM measurements. X-Ray adsorption experiments were performed at SPring-8.

References

1 (*a*) J. P. Wilcoxon and B. L. Abrams, *Chem. Soc. Rev.*, 2006, **35**, 1162; (*b*) J. D. MacKenzie and E. P. Bescher, *Acc. Chem. Res.*, 2007, **40**, 810; (*c*) S. G. Kwon and T. Hyeon, *Acc. Chem. Res.*, 2008, **41**, 1696.
2 D. L. Laslie-Pelecky and R. D. Rieke, *Chem. Mater.*, 1996, **8**, 1770.

3 (*a*) M. A. El-Sayed, *Acc. Chem. Res.*, 2001, **34**, 257; (*b*) D. Astruc, F. Lu and J. R. Aranzaes, *Angew. Chem., Int. Ed.*, 2005, **44**, 7852.
4 (*a*) M. Arai, Y. Takada and Y. Nishiyama, *J. Phys. Chem. B*, 1998, **102**, 1968; (*b*) M. Zhao and R. M. Crooks, *Angew. Chem., Int. Ed.*, 1999, **38**, 364; (*c*) J. W. Yoo, D. Hathcock and M. A. El-Sayed, *J. Phys. Chem. A*, 2002, **106**, 2049; (*d*) P. Concepción, A. Corma, J. Silvestre-Albero, V. Franco and J. Y. Chane-Ching, *J. Am. Chem. Soc.*, 2004, **126**, 5523; (*e*) K. Mori, T. Hara, T. Mizugaki, K. Ebitani and K. Kaneda, *J. Am. Chem. Soc.*, 2004, **126**, 10657.
5 (*a*) R. M. Crooks, M. Zhao, L. Sun, V. Chechik and L. K. Yeung, *Acc. Chem. Res.*, 2001, **34**, 181; (*b*) T. Mizugaki, M. Murata, S. Fukubayashi, T. Mitsudome, K. Jitsukawa and K. Kaneda, *Chem. Commun.*, 2008, 241.
6 R. S. Underhill and G. Liu, *Chem. Mater.*, 2000, **12**, 3633.
7 J. H. Ding and D. L. Gin, *Chem. Mater.*, 2000, **12**, 22.
8 (*a*) K. Mori, S. Kanai, T. Hara, T. Mizugaki, K. Ebitani, K. Jitsukawa and K. Kaneda, *Chem. Mater.*, 2007, **19**, 1249; (*b*) K. Mori, Y. Kondo, S. Morimoto and H. Yamashita, *Chem. Lett.*, 2007, **36**, 1068; (*c*) K. Mori, Y. Kondo, S. Morimoto and H. Yamashita, *J. Phys. Chem. C*, 2008, **112**, 2593; (*d*) K. Mori, K. Sugihara, Y. Kondo, T. Takeuchi, S. Morimoto and H. Yamashita, *J. Phys. Chem. C*, 2008, **112**, 16478.
9 (*a*) M. T. Reetz, A. Zonta, V. Vijayakrishnan and K. Schimossek, *J. Mol. Catal. A: Chem.*, 1998, **134**, 251; (*b*) X. Gao, K. M. K. Yu, K. Tam and S. C. Tsang, *Chem. Commun.*, 2003, 2998; (*c*) H. M. R. Garadimalla, D. Mandal, P. D. Stevens, M. Yen and Y. Gao, *Chem. Commun.*, 2005, 4432; (*d*) P. D. Stevens, G. Li, J. Fan, M. Yen and Y. Gao, *Chem. Commun.*, 2005, 4435.
10 (*a*) S. Sun, C. B. Murray, D. Weller, L. Folks and A. Moser, *Science*, 2000, **287**, 1989; (*b*) E. Shevchenko, D. Talapin, A. Kornowski, J. Kotzler, M. Haase, A. Rogach and H. Weller, *Adv. Mater.*, 2002, **12**, 287; (*c*) B. Jeyadevan, A. Hobo, K. Urakawa, C. N. Chinnasamy, K. Shinoda and K. Tohji, *J. Appl. Phys.*, 2003, **93**, 7574; (*d*) M. Nakaya, Y. Tsuchiya, K. Ito, Y. Oumi, T. Sano and T. Teranishi, *Chem. Lett.*, 2004, **33**, 130; (*e*) H. G. Bagaria, E. T. Ada, M. Shamsuzzoha, D. E. Nikles and D. T. Johnson, *Langmuir*, 2006, **22**, 7732; (*f*) V. Nandwana, K. E. Elkins, N. Poudyal, G. S. Chaubey, K. Yano and J. P. Liu, *J. Phys. Chem. C*, 2007, **111**, 4185.
11 (*a*) D.-Y. Wang, C.-H. Chen, H.-C. Yen, Y.-L. Lin, P.-Y. Huang, B.-J. Hwang and C.-C. Chen, *J. Am. Chem. Soc.*, 2007, **129**, 1538; (*b*) R. Wunder and J. Phillips, *J. Phys. Chem.*, 1994, **98**, 12329; (*c*) T. Teranishi and M. Miyake, *Chem. Mater.*, 1999, **11**, 3414.
12 C. Noguez and I. L. Garzón, *Chem. Soc. Rev.*, 2009, **38**, 757.
13 J. W. Long, M. S. Logan, C. P. Rhodes, E. E. Carpenter, R. M. Stroud and D. R. Rolison, *J. Am. Ceram. Soc.*, 2004, **126**, 16879.
14 (*a*) Y. Hou, H. Kondoh, T. Kogure and T. Ohta, *Chem. Mater.*, 2004, **16**, 5149.
15 J. M. Coey and D. Khalafalla, *Phys. Status Solidi A*, 1972, **11**, 229.
16 S. Mobilio and E. Burattini, *EXAFS and Near Edge Structure III*, ed. K. O. Hodgson, Springlar-Verlag, Berline, 1984, p. 222.
17 (*a*) X. Teng, D. Black, N. J. Watkins, Y. Gao and H. Yang, *Nano Lett.*, 2003, **3**, 261; (*b*) B. Ravel, E. E. Carpenter and V. G. Harris, *J. Appl. Phys.*, 2002, **91**, 8195; (*c*) V. E. Fertman, *Magnetic Fluids Guidebook: Properties and Applications*, Hemisphere Publishing Corporation, New York, 1990.
18 (*a*) E.-I. Negishi and F. Liu, In *Metal-Catalyzed Cross-Coupling Reactions*, ed. F. Diederich and P. J. Stang, Wiley-VCH, Weinheim, 1998; (*b*) J. P. Wolfe, S. Wagaw, J.-F. Marcoux and S. L. Buchwald, *Acc. Chem. Res.*, 1998, **31**, 805; (*c*) J. F. Hartwing, *Angew. Chem., Int. Ed.*, 1998, **37**, 2046; (*d*) V. Farina, *Adv. Synth. Catal.*, 2004, **346**, 1553.
19 (*a*) W. A. Herrmann, C. Brossmer, K. Öfele, C.-P. Reisinger, T. Priermeier, M. Beller and H. Fischer, *Angew. Chem., Int. Ed. Engl.*, 1995, **34**, 1844; (*b*) J. Dupont, M. Pfeffer and J. Osborn, *Eur. J. Inorg. Chem.*, 2001, 1917; (*c*) R. B. Bedford, *Chem. Commun.*, 2003, 1787.
20 M. Ohff, A. Ohff, M. E. van der Boom and D. Milstein, *J. Am. Chem. Soc.*, 1997, **119**, 11687.
21 (*a*) W. A. Herrmann, M. Elison, C. Ficher, C. Köcher and G. R. J. Artus, *Angew. Chem., Int. Ed. Engl.*, 1995, **34**, 2371; (*b*) W.A. Herrmann, K. Ofele, D. Von Preysing and S. K. Schneider, *J. Organomet. Chem.*, 2002, **41**, 1291.
22 (*a*) A. N. Cammidge and K. V. L. Crepy, *Chem. Commun.*, 2000, 1723; (*b*) J. Yin and S. L. Buchwald, *J. Am. Chem. Soc.*, 2000, **122**, 12051; (*c*) P. Kasak, K. Mereiter and M. Widhalm, *Tetrahedron: Asymmetry*, 2005, **16**, 3416; (*d*) M. Genov, A. Almorin and P. Espinet, *Chem.–Eur. J.*, 2006, **12**, 9346.
23 K. Sawai, R. Tatumi, T. Nakahodo and H. Fujiwara, *Angew. Chem., Int. Ed.*, 2008, **47**, 6917.

